Available online at www.sciencedirect.com
ScienceDirect
Food Research International 39 (2006) 1084–1091
FOOD RESEARCH INTERNATIONAL
www.elsevier.com/locate/foodres

Color measurement in $L^*a^*b^*$ units from RGB digital images

Katherine León [a], Domingo Mery [b,*], Franco Pedreschi [c], Jorge León [c]

[a] Departamento de Ingeniería Informática, Universidad de Santiago de Chile (USACH), Avenida Ecuador 3659, Santiago, Chile
[b] Departamento de Ciencia de la Computación, Pontificia Universidad Católica de Chile, Av. Vicuña Mackenna 4586(143), Macul, Santiago, Chile
[c] Departmento de Ciencia y Tecnología de Alimentos, Facultad Tecnológica, Universidad de Santiago de Chile (USACH), Av. Ecuador 3769, Santiago, Chile

Received 14 December 2005; accepted 11 March 2006

Abstract

The superficial appearance and color of food are the first parameters of quality evaluated by consumers, and are thus critical factors for acceptance of the food item by the consumer. Although there are different color spaces, the most used of these in the measuring of color in food is the $L^*a^*b^*$ color space due to the uniform distribution of colors, and because it is very close to human perception of color. In order to carry out a digital image analysis in food, it is necessary to know the color measure of each pixel on the surface of the food item. However, there are at present no commercial $L^*a^*b^*$ color measures in pixels available because the existing commercial colorimeters generally measure small, non-representative areas of a few square centimeters. Given that RGB digital cameras obtain information in pixels, this article presents a computational solution that allows the obtaining of digital images in $L^*a^*b^*$ color units for each pixel of the digital RGB image. This investigation presents five models for the RGB $\rightarrow L^*a^*b^*$ conversion and these are: linear, quadratic, gamma, direct, and neural network. Additionally, a method is suggested for estimating the parameters of the models based on a minimization of the mean absolute error between the color measurements obtained by the models, and by a commercial colorimeter for uniform and homogenous surfaces. In the evaluation of the performance of the models, the neural network model stands out with an error of only 0.93%. On the basis of the construction of these models, it is possible to find a $L^*a^*b^*$ color measuring system that is appropriate for an accurate, exacting and detailed characterization of a food item, thus improving quality control and providing a highly useful tool for the food industry based on a color digital camera.

Keywords: Color; RGB; $L^*a^*b^*$; Computer vision; Neural networks

1. Introduction

The aspect and color of the food surface is the first quality parameter evaluated by consumers and is critical in the acceptance of the product, even before it enters the mouth. The color of this surface is the first sensation that the consumer perceives and uses as a tool to accept or reject food. The observation of color thus allows the detection of certain anomalies or defects that food items may present (Abdullah, Guan, Lim, & Karim, 2004; Du & Sun, 2004; Hatcher, Symons, & Manivannan, 2004; Pedreschi, Aguilera, & Brown, 2000). The determination of color can be carried out by visual (human) inspection or by using a color measuring instrument. Although human inspection is quite robust even in the presence of changes in illumination, the determination of color is in this case, subjective and extremely variable from observer to observer. In order to carry out a more objective color analysis, color standards are often used as reference material. Unfortunately, their use implies a slower inspection and requires more specialized training of the observers. For there reasons it is recommendable to determine color through the use of color measuring instrumentation.

At present, color spaces and numerical values are used to create, represent and visualize colors in two and three dimensional space (Trusell, Saber, & Vrhel, 2005). Usually, the color of foods has been measured in $L^*a^*b^*$. The $L^*a^*b^*$, or CIELab, color space is an international standard

* Corresponding author. Tel.: +562 354 5820; fax: +562 354 4444.
E-mail addresses: dmery@ing.puc.cl, dmery@ieee.org (D. Mery).
URL: www.ing.puc.cl/~dmery (D. Mery).

0963-9969/$ - see front matter © 2006 Elsevier Ltd. All rights reserved.
doi:10.1016/j.foodres.2006.03.006

for color measurements, adopted by the Commission Internationale d'Eclairage (CIE) in 1976. L^* is the luminance or lightness component, which ranges from 0 to 100, and parameters a^* (from green to red) and b^* (from blue to yellow) are the two chromatic components, which range from −120 to 120 (Papadakis, Abdul-Malek, Kamdem, & Yam, 2000; Segnini, Dejmek, & Öste, 1999; Yam & Papadakis, 2004). The $L^*a^*b^*$ space is perceptually uniform, i.e., the Euclidean distance between two different colors corresponds approximately to the color difference perceived by the human eye (Hunt, 1991). In order to carry out a detailed characterization of the image of a food item and thus more precisely evaluated its quality, it is necessary to know the color value of each pixel of its surface. However, at present available commercial colorimeters measure $L^*a^*b^*$ only over a very few square centimeters, and thus their measurements are not very representative in heterogeneous materials such as most food items (Papadakis et al., 2000; Segnini et al., 1999). Colorimeters such as: (i) Minolta chroma meter; (ii) Hunter Lab colorimeter and (iii) Dr. Lange colorimeters are some of the instruments most used in the measurement of color, however they have the disadvantage that the surface to be measured must be uniform and rather small (~2 cm^2) which makes the measurements obtained quite unrepresentative and furthermore the global analysis of the food's surface becomes more difficult (Mendoza & Aguilera, 2004; Papadakis et al., 2000; Segnini et al., 1999).

In recent years, computer vision has been used to objectively measure the color of different foods since they provide some obvious advantages over a conventional colorimeter, namely, the possibility of analyzing of each pixel of the entire surface of the food, and quantifying surface characteristics and defects (Brosnan & Sun, 2004; Du & Sun, 2004). The color of many foods has been measured using computer vision techniques (Mendoza & Aguilera, 2004; Papadakis et al., 2000; Pedreschi, Mery, Mendoza, & Aguilera, 2004; Scanlon, Roller, Mazza, & Pritchard, 1994; Segnini et al., 1999). A computational technique with a combination of a digital camera, image processing software has been used to provide a less expensive and more versatile way to measure the color of many foods than traditional color-measuring instruments (Yam & Papadakis, 2004). With a digital camera it is possible to register the color of any pixel of the image of the object using three color sensors per pixel (Forsyth & Ponce, 2003). The most often used color model is the RGB model in which each sensor captures the intensity of the light in the red (R), green (G) or blue (B) spectrum, respectively. Today the tendency is to digitally analyze the images of food items in order to firstly carry out a point analysis, encompassing a small group of pixels with the purpose of detecting small characteristics of the object, and secondly to carry out a global analysis of the object under study such as a color histogram in order to analyze the homogeneity of the object, (Brosnan & Sun, 2004; Du & Sun, 2004). The use of color considerably improves high level image processing tasks (Mendoza & Aguilera, 2004; Pedreschi et al., 2004; Segnini et al., 1999). The published computational approaches that convert RGB into $L^*a^*b^*$ units use an absolute model with known parameters (Mendoza & Aguilera, 2004; Paschos, 2001; Segnini et al., 1999). In these works, the parameters are not estimated in a calibration process. However, the parameters of the models vary from one case to another because RGB is a non-absolute color space, i.e., the RGB color measurement depends on external factors (sensitivity of the sensors of the camera, illumination, etc.). Ilie and Welch (2005) reported that most cameras (even of the same type) do not exhibit consistent responses. This means, that the conversion from RGB to $L^*a^*b^*$ cannot be done directly using a standard formula, like a conversion from centimeters to inches.

This article presents a methodology for obtaining accurate device-independent $L^*a^*b^*$ color units from device-dependent RGB color units captured by a digital color camera. A similar methodology was published in Hardeberg, Schmitt, Tastl, Brettel, and Crettez (1996), in which a color chart[1] containing several samples with known $L^*a^*b^*$ measurements was used for the calibration of a scanner. However, details of the used models are not given in the paper and the possible wear of the color in the chart is not considered. In order to avoid the mentioned problems, the solution presented in this paper is based on modeling the transformation of coordinates of the RGB color space into coordinates of the $L^*a^*b^*$ color space so that the values delivered by the model are as similar as possible to those delivered by a colorimeter over homogenous surfaces.

Although the methodology presented in our paper is general, i.e., it can be used in every computer vision system, we must clarify that the results obtained after the calibration for one system (e.g., system A) cannot be used for another system (e.g., system B). The reason is because the calibration obtained for computer vision system A is applicable only to the specific camera and illumination setups used by system A. This means that computer vision system B requires a new calibration procedure that considers the characteristics of the camera and illumination used by system B.

This study uses five models to carry out the RGB → $L^*a^*b^*$ transformation: direct, gamma, linear, quadratic and neural. This article presents the details of each model, their performance, and their advantages and disadvantages. The purpose of this work was to find a model (and estimate its parameters) for obtaining $L^*a^*b^*$ color measurements from RGB measurements.

2. Materials and methods

The images used in this work were taken with the following image acquisition system (see Fig. 1):

[1] A color chart is a piece of paper painted in such a way that the color surface shows an uniform distributed color.

- Canon PowerShot G3 color digital camera with 4 Mega Pixels of resolution, placed vertically at a distance of 22.5 cm from the samples. The angle between the axis of the lens and the sources of illumination is approximately 45°.
- Illumination was achieved with 4 Philips, Natural Daylight 18 W fluorescent lights (60 cm in length), with a color temperature of 6500 K, and a color index (Ra) close to 95%.
- The illuminating tubes and the camera were placed in a wooden box the interior walls of which were painted black to minimize background light.
- The images were taken at maximum resolution (2272×1704 pixels) and connected to the USB port of a Pentium IV, 1200 MHz computer.
- The settings of the camera used in our experiments are summarized in Table 1.

In order to calibrate the digital color system, the color values of 32 color charts were measured (see some charts in Fig. 2). Each color chart was divided into 10 regions as shown in Fig. 3. In each region, the $L^*a^*b^*$ color values were measured using a Hunter Lab colorimeter. Additionally, a RGB digital image was taken of each chart, and the R, G and B color values of the corresponding regions were measured using a Matlab program which computes the mean values for each color value in each region according to the 10 masks illustrated in Fig. 3. Thus, 320 RGB measurements were obtained as were their corresponding 320 $L^*a^*b^*$ measurements (from the colorimeter).

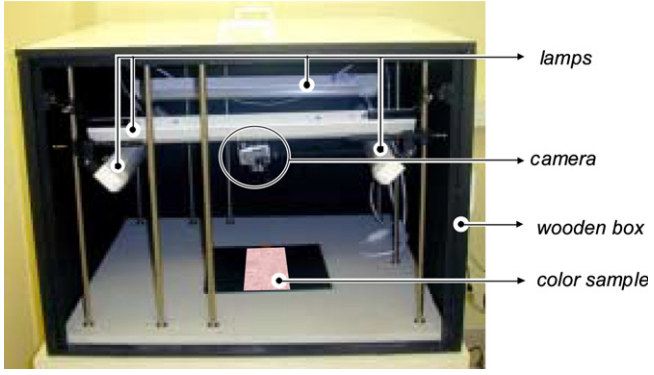

Fig. 1. Image acquisition system.

Table 1
Camera's setup

Variable	Value
Focal distance	20.7 mm
Zoom	9
Flash	Off
Iso velocity	100
White balance	Fluorescence H
Operation mode	Manual
Aperture Av	f/8.0
Exposure Tv	1/15 s
Quality	Raw
Macro	On

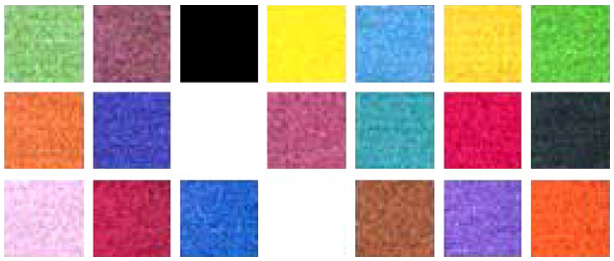

Fig. 2. Array showing 21 of the 32 color charts used in the calibration process.

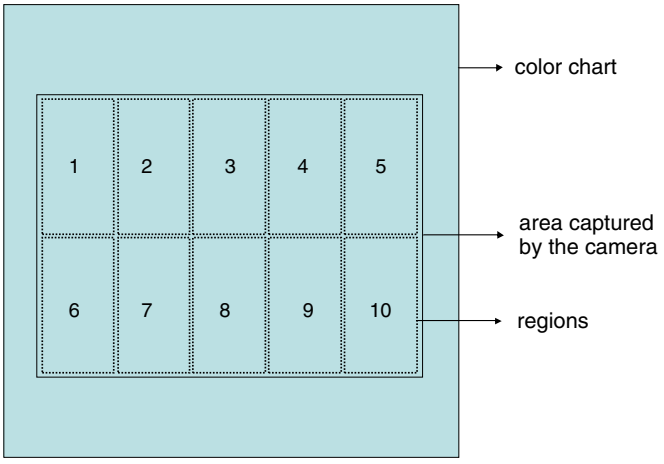

Fig. 3. The color of 10 regions of each chart is measured.

Prior to the construction of the different models, the samples were divided. A set of 62.5% of the samples (200 measurements) RGB and $L^*a^*b^*$ measurements were used for training purposes, and the remaining 37.5% of the samples (120 measurements) were set aside for testing. This division was used for the first four models. The fourth, neural network model is a special case, as for this model, 80% of the samples (256 measurements) were used for training, 10% (32 measurements) were used for validation, and the remaining 10% (32 measurements) were used for testing. For this last case, the crossed validation technique (Mitchell, 1997) was used in order to ensure the generality of the neural network.

The methodology used for estimating the RGB $\rightarrow$ $L^*a^*b^*$ transformation consists of two parts (see Fig. 4 and the nomenclature used in Table 2):

(i) Definition of the model: The model has parameters $\theta_1, \theta_2, \ldots \theta_m$ whose inputs are the RGB variables obtained from the color digital image of a sample, and whose outputs are the $L^*a^*b^*$ variables estimated from the model, (see R, G, B and $\hat{L}^*$, $\hat{a}^*$, $\hat{b}^*$, respectively, in Fig. 4); and

(ii) Calibration: The parameters $\theta_1, \theta_2, \ldots, \theta_m$ for the model are estimated on the basis of the minimization of the mean absolute error between the estimated

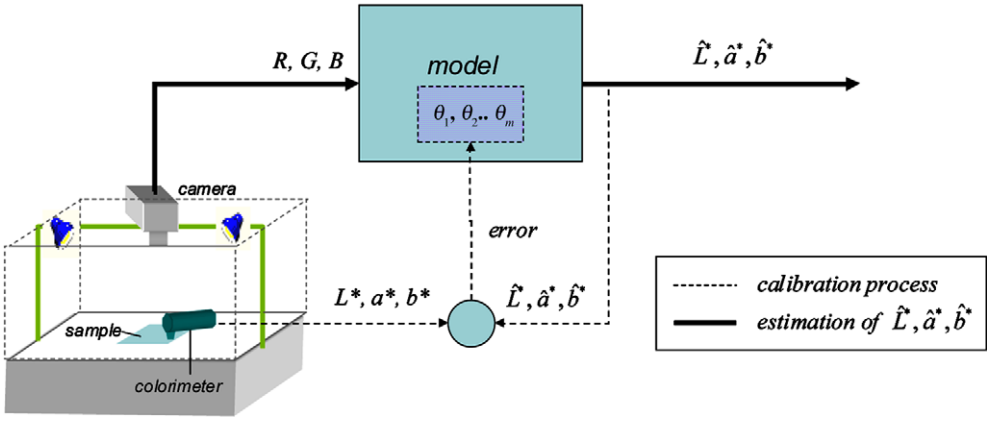

Fig. 4. Estimate of $L^*a^*b^*$ values on the basis of RGB measurements.

Table 2
Nomenclature used

Variable	Description
L^*	Value of L^* measured with a colorimeter
a^*	Value of a^* measured with a colorimeter
b^*	Value of b^* measured with a colorimeter
$\hat{L}^*$	Value of L^* obtained with the model
$\hat{a}^*$	Value of a^* obtained with the model
$\hat{b}^*$	Value of b^* obtained with the model
R	Value of R (red) measured from the digital image
G	Value of G (green) measured from the digital image
B	Value of B (blue) measured from the digital image
e_L	Error in the estimate of L^*
e_a	Error in the estimate of a^*
e_b	Error in the estimate of b^*

variables (model output) $\hat{L}^*$, $\hat{a}^*$, $\hat{b}^*$ and the L^*, a^*, b^* variables (measured from the sample used in i) through the use of a colorimeter.

Once the system has been calibrated it is possible to infer the $L^*a^*b^*$ values on the basis of the RGB measurements from the camera without having to use the colorimeter (see continuous line in Fig. 4).

The mean normalized error in the estimate of each of the $L^*a^*b^*$ variables is obtained by comparing colorimeter measurements (L^*, a^*, b^*) with model estimates ($\hat{L}^*$, $\hat{a}^*$, $\hat{b}^*$):

$$e_L = \frac{1}{N}\sum_{i=1}^{N}\frac{|L_i^* - \hat{L}_i^*|}{\Delta L},$$
$$e_a = \frac{1}{N}\sum_{i=1}^{N}\frac{|a_i^* - \hat{a}_i^*|}{\Delta a}, \quad (1)$$
$$e_b = \frac{1}{N}\sum_{i=1}^{N}\frac{|b_i^* - \hat{b}_i^*|}{\Delta b}.$$

These errors are calculated by averaging N measurements for $i = 1, \ldots, N$. The errors have been normalized according to the range of each of the scales. As the measurements are in the intervals $0 \leqslant L^* \leqslant 100$, $-120 \leqslant a^* \leqslant -120$ and $-120 \leqslant b^* \leqslant 120$, the range used is $\Delta L = 100$ and $\Delta a = \Delta b = 240$. In order to evaluate the performance of the model used, the mean error is calculated:

$$\bar{e} = \frac{e_b + e_b + e_b}{3}. \quad (2)$$

The problem of estimating model parameters can be posed as follows. Let $\mathbf{f}$ be the function which transforms the coordinates (R, G, B) in $(\hat{L}^*, \hat{a}^*, \hat{b}^*)$:

$$(\hat{L}^*, \hat{a}^*, \hat{b}^*) = \mathbf{f}(\boldsymbol{\theta}, R, G, B), \text{ or } \begin{bmatrix}\hat{L}^*\\ \hat{a}^*\\ \hat{b}^*\end{bmatrix} = \begin{bmatrix}f_L(\boldsymbol{\theta}, R, G, B)\\ f_a(\boldsymbol{\theta}, R, G, B)\\ f_b(\boldsymbol{\theta}, R, G, B)\end{bmatrix}, \quad (3)$$

where $\boldsymbol{\theta} = [\theta_1\theta_2 \ldots \theta_m]^{\mathrm{T}}$ is the parameter vector for model $\mathbf{f}$. Therefore, $\boldsymbol{\theta}$ must be estimated such that the mean error $\bar{e}$ is minimized in (2). In this paper, minimization is carried out using Matlab software (MathWorks, 2000). When $\mathbf{f}$ is linear, a direct linear regression method is used for the parameters. Nonetheless, for non-linear functions it is necessary to use iterative methods such as the fminsearch function, which searches for the minimum of the target function based on a gradient method.

2.1. Construction of models

This section describes the five models that can be used for the RGB $\rightarrow L^*a^*b^*$ transformation: linear, quadratic, direct, gamma and neural networks.

2.1.1. Linear Model

In this, the simplest model of all, the RGB $\rightarrow L^*a^*b^*$ transformation is a linear function of the (R, G, B) variables:

$$\begin{bmatrix}\hat{L}^*\\ \hat{a}^*\\ \hat{b}^*\end{bmatrix} = \begin{bmatrix}M_{11} & M_{12} & M_{13} & M_{14}\\ M_{21} & M_{22} & M_{23} & M_{24}\\ M_{31} & M_{32} & M_{33} & M_{34}\end{bmatrix}\begin{bmatrix}R\\ G\\ B\\ 1\end{bmatrix}. \quad (4)$$

The following is an explanation of how the parameters of the first row of matrix **M** in (4) are obtained; the same explanation is valid for the other rows: We first must define

- The parameters vector for the model

$$\boldsymbol{\theta} = [M_{11} \quad M_{12} \quad M_{13} \quad M_{14}]^{\mathrm{T}}, \tag{5}$$

- The input matrix with N measurements of R, G, B

$$\mathbf{X} = \begin{bmatrix} R_1 & G_1 & B_1 & 1 \\ : & : & : & : \\ R_N & G_N & B_N & 1 \end{bmatrix}, \tag{6}$$

- And the output vector with the N measurements of L^*

$$\mathbf{y} = [L_1^* \quad \ldots \quad L_N^*]^{\mathrm{T}}, \tag{7}$$

thus the estimate of L^*, obtained from the minimization of the norm between measurements and estimated $\|\mathbf{y} - \hat{\mathbf{y}}\|$, is defined by (Stöderström & Stoica, 1989):

$$\hat{\mathbf{y}} = \mathbf{X}\boldsymbol{\theta}, \tag{8}$$

where

$$\boldsymbol{\theta} = [\mathbf{X}^{\mathrm{T}}\mathbf{X}]^{-1}\mathbf{X}^{\mathrm{T}}\mathbf{y}. \tag{9}$$

The advantage of this model is that it is direct and its solution is not obtained through iterations.

2.1.2. Quadratic model

This model considers the influence of the square of the variables (R, G, B) on the estimate of the values $(\hat{L}^*, \hat{a}^*, \hat{b}^*)$ values:

$$\begin{bmatrix} \hat{L}^* \\ \hat{a}^* \\ \hat{b}^* \end{bmatrix} = \begin{bmatrix} M_{11} & M_{12} & M_{13} & M_{14} & M_{15} & M_{16} & M_{17} & M_{18} & M_{19} & M_{1,10} \\ M_{21} & M_{22} & M_{23} & M_{24} & M_{25} & M_{26} & M_{27} & M_{28} & M_{29} & M_{2,10} \\ M_{31} & M_{32} & M_{33} & M_{34} & M_{35} & M_{36} & M_{37} & M_{38} & M_{39} & M_{3,10} \end{bmatrix} \begin{bmatrix} R \\ G \\ B \\ RG \\ RB \\ GB \\ R^2 \\ G^2 \\ B^2 \\ 1 \end{bmatrix}. \tag{10}$$

The estimate of the parameters of matrix **M** is carried out in the same manner as in the previous model, as this model, as can be seen in (10), is linear in the parameters in spite of being quadratic in the variables. The first row requires the following definitions:

- The parameter vector for the model

$$\boldsymbol{\theta} = [M_{11} \quad M_{12} \quad \ldots \quad M_{1,10}]^{\mathrm{T}}, \tag{11}$$

- The input matrix with N measurements of (R, G, B)

$$\mathbf{X} = \begin{bmatrix} R_1 & G_1 & B_1 & R_1G_1 & R_1B_1 & G_1B_1 & R_1^2 & G_1^2 & B_1^2 & 1 \\ : & : & : & : & : & : & : & : & : & : \\ R_N & G_N & B_N & R_NG_N & R_NB_N & G_NB_N & R_N^2 & G_N^2 & B_N^2 & 1 \end{bmatrix}, \tag{12}$$

and the output vector with N measurements of L^* as defined in (7). The estimate of L^* is likewise defined using Eqs. (8) and (9).

2.1.3. Direct model

This model carries out the RGB → $L^*a^*b^*$ transformation in two steps (Hunt, 1991):

- The first step carries out the RGB → XYZ transformation:

$$\begin{bmatrix} X \\ Y \\ Z \end{bmatrix} = \begin{bmatrix} M_{11} & M_{12} & M_{13} & M_{14} \\ M_{21} & M_{22} & M_{23} & M_{24} \\ M_{31} & M_{32} & M_{33} & M_{34} \end{bmatrix} \begin{bmatrix} R \\ G \\ B \\ 1 \end{bmatrix}, \tag{13}$$

- And the second step carries out the XYZ → $L^*a^*b^*$ transformation:

$$\begin{aligned} \hat{L}^* &= \begin{cases} 116\left(\frac{Y}{Y_n}\right)^{1/3} - 16 & \text{if } \frac{Y}{Y_n} > 0.008856 \\ 903.3\left(\frac{Y}{Y_n}\right) & \text{if } \frac{Y}{Y_n} \leqslant 0.008856 \end{cases} \\ \hat{a}^* &= 500\left[\left(\frac{X}{X_n}\right)^{1/3} - \left(\frac{Y}{Y_n}\right)^{1/3}\right], \\ \hat{b}^* &= 200\left[\left(\frac{Y}{Y_n}\right)^{1/3} - \left(\frac{Z}{Z_n}\right)^{1/3}\right], \end{aligned} \tag{14}$$

where X_n, Y_n, Z_n are the valued of the reference blank, and M_{ij} are the elements of a linear transformation matrix **M** between the spaces RGB and XYZ.

In order to carry out this transformation, a function **f**, such as is shown in (3) is defined from (13) and (14). This function receives as parameters the elements of the transformation matrix **M**, as well as the RGB and $L^*a^*b^*$ data from the samples previously obtained by digital camera and the colorimeter. The parameters for **f** are obtained

through some iterative method such as the one previously described.

2.1.4. Gamma model

This model has had added to it the *gamma factor* (Forsyth & Ponce, 2003), in order to correct the RGB values obtained from the digital camera, thus obtaining a better calibration of the transformation model.

The difference between this model and the previous one is the addition of *gamma correction* parameters which correspond to the values α_1, α_2 and the value of the *gamma factor*, γ:

$$R_\gamma = \left(\frac{R+\alpha_1}{\alpha_2}\right)^\gamma, \quad G_\gamma = \left(\frac{G+\alpha_1}{\alpha_2}\right)^\gamma, \quad B_\gamma = \left(\frac{B+\alpha_1}{\alpha_2}\right)^\gamma. \tag{15}$$

The values of the (X, Y, Z) are obtained by using

$$\begin{bmatrix} X \\ Y \\ Z \end{bmatrix} = \begin{bmatrix} M_{11} & M_{12} & M_{13} \\ M_{21} & M_{22} & M_{23} \\ M_{31} & M_{32} & M_{33} \end{bmatrix} \begin{bmatrix} R_\gamma \\ G_\gamma \\ B_\gamma \end{bmatrix}, \tag{16}$$

and the estimation of the $(\hat{L}^*, \hat{a}^*, \hat{b}^*)$ values is carried out using (14) and the estimation of the parameters of the model is carried out in the same manner as used for the direct model describe above.

2.1.5. Neural network

Neural networks can be more effective if the network input and output data are previously treated. Prior to training, it is very useful to normalize the data so that they always lie within some specified range. This was done for the range [0 a 1] according to:

$$x_i = \frac{x_i - x_{\min}}{x_{\max} - x_{\min}}, \tag{17}$$

where x_i, $x_{\min}$, $x_{\max}$ are, respectively, the original, minimum and maximum values that the input variable that is being normalized can have.

The parameters of the neural network used are (see Fig. 5):

- The input layer uses one neuron for each color value, in other words, 3 neurons are used. The output layer also uses 3 layers as each of these will give a different color value for: $(\hat{L}^*, \hat{a}^*, \hat{b}^*)$.

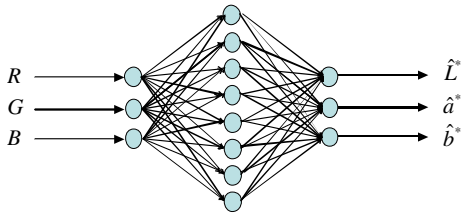

Fig. 5. Architecture of the neural network used.

- In order to choose the optimum number of neurons for the hidden layer, training starts with 5 neurons and goes increasing. The best performance, without overtraining, is achieved with 8 neurons (Haykin, 1994).
- Only one hidden layer is used because according to (Hornick, Stinchcombe, & White, 1989), all training carried out with two or more layers can be achieved with only one layer if the number of neurons in the layer is varied.
- During the training of the neural network, *Early Stopping* of neural network toolbox of Matlab was used in order to be able to exhaustively examine the behavior of error in the training, and stop it optimally.

3. Results and discussion

It is important to highlight the almost inexistent differences between error in training and error during testing, especially when considering that the samples with which the models were tested had not been seen during training. This is evidence that the five models used are capable of *generalizing* what was learned during the training stages. Table 3 presents the errors for each of the models.

The model that shows the best performance in the calculation of $L^*a^*b^*$ is the neural network, with an error of 0.93% and a standard deviation of 1.25, which ensures good performance for future tests. The quadratic model is the second best with calculation errors in 1.23% of the total samples, and a standard deviation of 1.50. It should be noted that one advantage of the quadratic model over the neural network model is that its training is not iterative, in other words the estimate of the parameters of the model is carried out directly (see Eq. (9)).

Another important factor to consider when comparing the performance of the models is execution time during the testing phase. Testing was carried out on a Pentium IV computer with a 1200 MHz processor. The direct and gamma models are the fastest, and always achieve results in less than one second. The neural network model, which achieved the best results in terms of the calculation of the $L^*a^*b^*$ values, finished in 1.21 s.

Fig. 6 shows the graphs of real values and estimated values for the two best models (quadratic and neural network), and there is evidently a great deal of similarity between the values estimated with the models and the real values of the variables yielding correlation coefficients grater than 0.99.

Table 3
Errors in calculating $L^*a^*b^*$

Model	Training		Test		Total	
	$\bar{e}$ (%)	σ	$\bar{e}$ (%)	σ	$\bar{e}$ (%)	σ
Linear	2.18	2.36	2.17	2.41	2.18	2.38
Quadratic	1.22	1.42	1.26	1.62	1.23	1.50
Direct	4.90	8.23	4.98	8.02	4.94	8.15
Gamma	3.56	4.20	3.49	4.46	3.53	4.30
Neural network	0.95	1.28	0.87	1.22	0.93	1.25

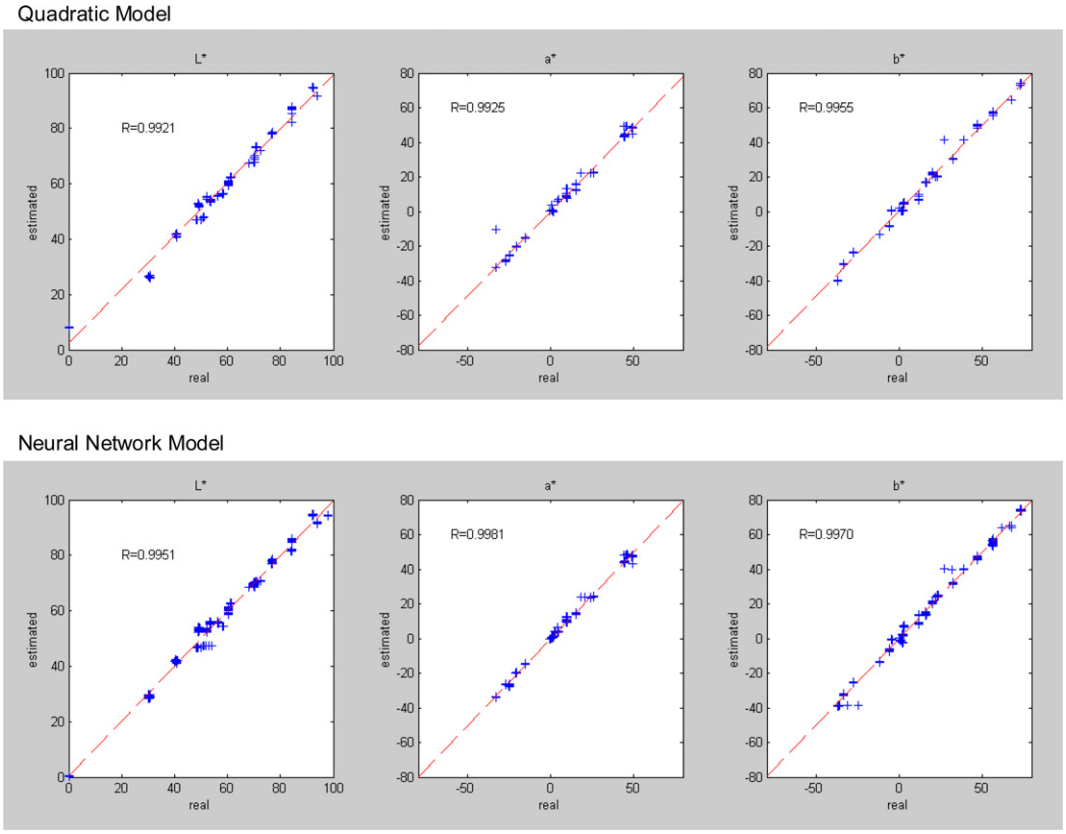

Fig. 6. Estimate of $L^*a^*b^*$ values for quadratic and neural network models.

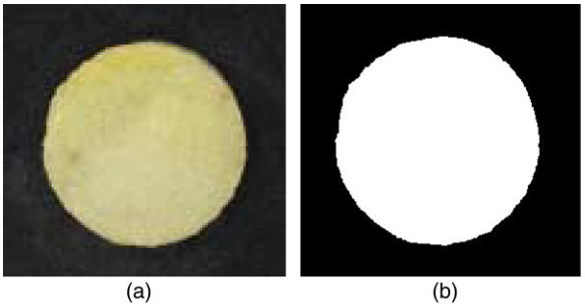

Instrument	L*	a*	b*
Hunter Lab	61.7	-1.7	26.6
Digital Image	66.9	-1.3	27.3

(a) (b) (c)

Fig. 7. Estimate of $L^*a^*b^*$ values of a potato chips: (a) RGB image; (b) segmented image after Mery and Pedreschi (2005); (c) $L^*a^*b^*$ measures using a commercial colorimeter and our approach.

In order to show the capability of the proposed method, the color of a potato chip was measured using both a Hunter Lab colorimeter and our approach. The colorimeter measurement was obtained by averaging 12 measurements (in 12 different places of the surface of the chip), whereas the measurement using the digital color image was estimated by averaging all pixels of the surface image. The results are summarized in Fig. 7. The error calculated after Eq. (2) is only 1.8%.

4. Conclusions

Five models were built that are able to measure color in $L^*a^*b^*$ units and simultaneously measure the color of each pixel on the target surface. This is not the case with conventional colorimeters. The best results were achieved with the quadratic and neural network model, both of which show small errors (close to 1%). With respect to the neural network it was demonstrated that with a correct selection of parameters and good architecture it is possible to solve problems such as the one addressed in this work.

This work has developed a tool for high-resolution $L^*a^*b^*$ color measurement. This system of color measurement is very useful in the food industry because a large amount of information can now be obtained from measurements at the pixel level, which allows a better characterization of foods and thus improves quality control.

In the future it is hoped that three separate neural networks can be implemented, one for each output required by this problem. Likewise, it would be interesting to

determine what would happen if the number of RGB values was augmented because in neural networks, larger amounts of data for training translate into results that are closer to the expected values, thus minimizing error.

Acknowledgements

Authors acknowledge financial support from FONDECYT Project No. 1030411.

References

Abdullah, M. Z., Guan, L. C., Lim, K. C., & Karim, A. A. (2004). The applications of computer vision and tomographic radar imaging for assessing physical properties of food. *Journal of Food Engineering, 61*, 125–135.

Brosnan, T., & Sun, D. (2004). Improving quality inspection of food products by computer vision – a review. *Journal of Food Engineering, 61*, 3–16.

Du, C., & Sun, D. (2004). Recent developments in the applications of image processing techniques for food quality evaluation. *Trends in Food Science and Technology, 15*, 230–249.

Forsyth, D., & Ponce, J. (2003). *Computer vision: a modern approach*. New Jersey: Prentice Hall.

Hardeberg, J. Y., Schmitt, F., Tastl, I., Brettel, H., & Crettez, J.-P. (1996). In *Proceedings of 4th Color Imaging Conference: Color Science, Systems and Applications*, Scottsdale, Arizona, Nov (pp. 108–113).

Hatcher, D. W., Symons, S. J., & Manivannan, U. (2004). Developments in the use of image analysis for the assessment of oriental noodle appearance and color. *Journal of Food Engineering, 61*, 109–117.

Haykin, S. (1994). *Neuronal networks – a comprehensive foundation*. New York: Macmillan College Publishing. Inc.

Hornick, K., Stinchcombe, M., & White, H. (1989). Multilayer feedforward networks are universal approximators. *Neural Networks, 2*, 359–366.

Hunt, R. W. G. (1991). *Measuring color* (2nd ed.). New York: Ellis Horwood.

Ilie, A., & Welch, G. (2005). Ensuring color consistency across multiple cameras. In Proceedings of the tenth IEEE international conference on computer vision (ICCV-05), Vol. 2, 17–20 Oct (pp. 1268–1275).

MathWorks (2000). Optimization toolbox for use with Matlab: users guide. The MathWorks Inc.

Mendoza, F., & Aguilera, J. M. (2004). Application of image analysis for classification of ripening bananas. *Journal of Food Science, 69*, 471–477.

Mery, D., & Pedreschi, F. (2005). Segmentation of colour food images using a robust algorithm. *Journal of Food Engineering, 66*(3), 353–360.

Mitchell, T. M. (1997). *Machine learning*. Boston: McGraw Hill.

Papadakis, S. E., Abdul-Malek, S., Kamdem, R. E., & Yam, K. L. (2000). A versatile and inexpensive technique for measuring color of foods. *Food Technology, 54*(12), 48–51.

Paschos, G. (2001). Perceptually uniform color spaces for color texture analysis: an empirical evaluation. *IEEE Transactions on Image Processing, 10*(6), 932–937.

Pedreschi, F., Aguilera, J. M., & Brown, C. A. (2000). Characterization of food surfaces using scale-sensitive fractal analysis. *Journal of Food Process Engineering, 23*, 127–143.

Pedreschi, F., Mery, D., Mendoza, F., & Aguilera, J. M. (2004). Classification of potato chips using pattern recognition. *Journal of Food Science, 69*(6), E264–E270.

Scanlon, M. G., Roller, R., Mazza, G., & Pritchard, M. K. (1994). Computerized video image analysis to quantify colour of potato chips. *American Potato Journal, 71*, 717–733.

Segnini, S., Dejmek, P., & Öste, R. (1999). A low cost video technique for colour measurement of potato chips. *Food Science and Technology-Lebensmittel-Wissenschaft und Technologie, 32*(4), 216–222.

Stöderström, T., & Stoica, P. (1989). *System identification*. New York: Prentice-Hall.

Trusell, H. J., Saber, E., & Vrhel, M. (2005). Color image processing. *IEEE Signal Processing Magazine, 22*(1), 14–22.

Yam, K. L., & Papadakis, S. (2004). A simple digital imaging method for measuring and analyzing color of food surfaces. *Journal of Food Engineering, 61*, 137–142.